Gradstein, F. M., Ludden, J. N., et al., 1992
Proceedings of the Ocean Drilling Program, Scientific Results, Vol. 123

7. EVOLUTION OF A MIOCENE CALCICLASTIC TURBIDITE DEPOSITIONAL SYSTEM[1]

Gregory R. Simmons[2]

ABSTRACT

A middle to upper Miocene turbidite depositional system exists at Site 765 in the southeastern Argo Abyssal Plain, along the northwest margin of Australia. Turbidites consist predominantly of planktonic calcareous components. Textural, mineralogical, bedding, and downhole logging trends within the system support the idea of a rapid progradation of the turbidite system in the middle to late Miocene. The onset of abundant turbidity currents into the area is attributed to changes in oceanographic conditions that accompanied the progressive lowering of sea level associated with major continental ice build-up on Antarctica. These data, in conjunction with seismic stratigraphy, support the existence of two major depositional pulses. Gradual retrogradation of the system occurred in latest Miocene time, coincident with the subsequent rising of sea level. Retrogradation of the system was overwhelmed by massive slope failures during the Pliocene, presumably triggered by earthquakes associated with the progressive Miocene–Pliocene collision of the Australian margin and the Sunda-Banda Arc.

INTRODUCTION

Calcareous turbidites are abundant within the Neogene section at Site 765, located in the southeastern Argo Abyssal Plain (Fig. 1). A turbidite depositional system existed here during middle to late Miocene time. Turbidity currents were a common sedimentary process throughout the Cenozoic and Cretaceous at Site 765, but turbidites within the Miocene series exhibit a systematic pattern having decipherable evolutionary trends. The intention of this post-cruise investigation was to document the growth history of the middle to late Miocene turbidite depositional system at Site 765, herein referred to as the "turbidite sequence," and to relate that history to the outside controlling factors that governed growth of the system. The investigation involves textural, bedding, and mineralogical analyses in conjunction with a synthesis of shipboard results (Ludden, Gradstein, et al., 1990). A LAB-TEC 100 particle-size analyzer was used for this investigation. The same instrument is available aboard the *JOIDES Resolution*. Included here are some comments about the performance of the LAB-TEC 100, which is compared with more traditional techniques also employed in this investigation and aboard the *JOIDES Resolution*.

REGIONAL GEOLOGY

The Argo Abyssal Plain (Fig. 1) is a thin sliver of old oceanic crust in the northeastern corner of the Indian Ocean, between northwestern Australia and the Sunda Arc. Subduction of the abyssal plain into the Java Trench is driving convergence of Australia and the Sunda Arc. The Neogene sediments of the Argo Abyssal Plain were likely influenced by the progressive Miocene–Pliocene collision between the Australian margin and the Sunda-Banda Arc (Carter et al., 1976) in influx of volcanic arc-derived materials and tectonic triggering of redepositional events.

Site 765 is located in the southeastern Argo Abyssal Plain on a starved passive margin off northwest Australia (Fig. 1). The site is situated ~75 km north of the continent/ocean boundary and sits in front of Swan Canyon, a reentrant bisecting Australia's Northwest Sheer and the marginal Exmouth Plateau. Swan Canyon and similar reentrants probably funneled mostly marginal marine materials from the Northwest Shelf and the Exmouth Plateau into the Argo Abyssal Plain during the Neogene. Site 765 is thought to have existed well below the calcite compensation depth (CCD) for most of its history, particularly through the Cenozoic. During Leg 122, a transect was cored (Sites 759 through 761 and 764) across the Wombat Plateau, a small subplateau on the northern edge of the Exmouth Plateau (Haq, von Rad, O'Connell, et al., 1990). From this transect, we recovered Upper Cretaceous to Cenozoic foraminifer and nannofossil oozes unconformably overlying Triassic shallow marine and coastal facies.

DESCRIPTION OF TURBIDITE SEQUENCE AND ITS BOUNDARIES

The following is a discussion of shipboard observations (Ludden, Gradstein, et al., 1990) centered on the upper and middle Miocene calcareous turbidites designated as lithologic Subunits IIA and IIB, which were recovered from 189 to 460 m below the seafloor (mbsf) at Site 765 (Fig. 2). These turbidites (5 to 200 cm thick) are typically sandy at the base and fine upward to dominantly clay- and silt-sized particles. These commonly include a thin quartzose base (<2 cm thick), but are principally composed of whole and broken foraminifers, additional calcareous fragments, nannofossils, and clays. Primary sedimentary structures normally associated with turbidites and that allow internal differentiation (e.g., facies A, B, C, D, and E; Bouma, 1962) are common only in Subunit IIB. The sediments of Subunit IIA are comparatively unlithified. The relative absence of primary sedimentary structures is attributed more to poor preservation during coding and handling than to any significant change in sedimentary processes between the subunits. Interbedded, clayey pelagic intervals are rare in Subunit IIA, but are common within Subunit IIB. The pelagic intervals are typically dark gray claystones containing as much as 20% to 30% fine sand-sized to coarse silt-sized glass and/or quartz. Common authigenic dolomite was noted as well. Maximum thickness of the pelagic intervals in Subunit IIB increases downward from 6 to 20 cm.

As might be expected, reworking includes microfossils older than the time of deposition. The oldest planktonic foraminifers are Late Cretaceous. The abundance of calcareous benthic foraminifers is generally low. Benthic assemblages typically range from upper to middle bathyal depths. Reworking of even older materials occurs within debris-flow deposits immediately underlying and overlying the turbidite sequence. These debris-flow deposits are matrix-supported conglomerates that consist primar-

[1] Gradstein, F. M., Ludden, J. N., et al., 1992. *Proc. ODP, Sci. Results,* 123: College Station, TX (Ocean Drilling Program).

[2] Department of Oceanography, Texas A&M University, College Station, TX 77843, U.S.A.

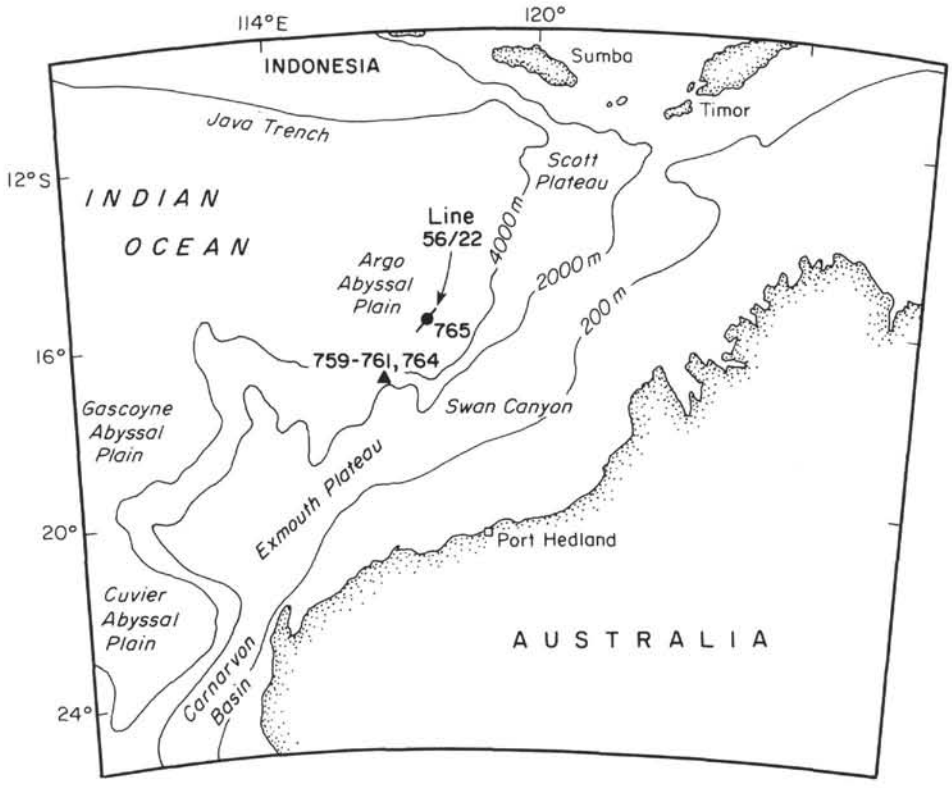

Figure 1. Location of Site 765, Argo Abyssal Plain, and track of BMR seismic Line 56/22. Modified from Ludden, Gradstein,et al. (1990).

ily of intraformational components, as well as some obviously allochthonous pebbles. Nannofossil ages of these pebbles range from Late Cretaceous to Middle Jurassic.

Underlying the turbidite sequence, Subunit IIC (Fig. 2) consists of a single turbidite (>225 cm thick) that overlies a disturbed, matrix-supported conglomerate (>350 cm thick). Farther down the section, in Subunit IIIA, calcareous turbidites (30–500 cm thick) are interbedded with clayey pelagic intervals (20–175 cm thick).

Overlying the turbidite sequence is Subunit IC (Fig. 2), which consists largely of calcareous turbidites (5–65 cm thick) similar to those in Subunits IIA and IIB. These turbidites are increasingly finer-grained upward, and interbedded pelagic intervals (1–25 cm thick) are increasingly abundant. Concomitant with this apparent retrogradation was an increasing occurrence and magnitude of massive redepositional events involving slumps, debris flows, and turbidity currents. Subunit IB consists almost entirely of massive sediment gravity-flow deposits up to 42.5 m thick. Farther up the section, Subunit IA consists of alternating fine-grained calcareous turbidites (10–200 cm thick) and intervals of clayey siliceous ooze (5–120 cm thick).

The turbidite sequence corresponds with seismic sequences 3, 4, and 5 (Figs. 2 and 3). The upper boundary of sequence 3 is near a lower Pliocene hiatus(?) within Subunit IC. This sequence boundary is locally onlapped, supporting an interpretation of a hiatus. The lower boundary of sequence 5, at the base of Subunit IIC, is a regional seismic unconformity. Sequences 3 and 4 are characterized by parallel to subparallel, generally low-amplitude reflections having moderate continuity. Gently mounded features exist locally. No obvious lithologic break corresponds to the high-amplitude boundary between sequences 3 and 4. The Shipboard Scientific Party speculated that it was a diagenetic boundary related to increased lithification within the turbidite sequence. Here, I identify an apparent depositional break at 290 mbsf, to which this seismic sequence boundary may tie. Sequence 5 is characterized by continuous, parallel, high-amplitude reflections related to lithologic availability within Subunit IIB.

The total gamma-ray counts fluctuate 10 to 20 API units locally in the turbidite sequence (Fig. 2), presumably in response to lithologic variability; however, only thicker beds tie directly to individual peaks and troughs. Vertical resolution of the gamma-ray tool is 46 cm (C. Broglia, pers. comm., 1991). Maximum and minimum gamma-ray values through the turbidite sequence occur over a short transition between 360 and 420 mbsf in Subunit IIB and lowermost Subunit IIA. After leveling off, above the short transition, the average gamma-ray values gradually increase upward through Subunits IIA and IC.

Magnetic susceptibility is generally low through the turbidite sequence (Fig. 2). Distinctive peaks occur primarily above 200 mbsf, near the top of Subunit IIA, and below 450 mbsf, near the base of Subunit IIB. These susceptibility peaks correspond to clay-rich pelagic intervals. Note that zero susceptibility corresponds to intervals of no recovery. In a few instances, a one-to-one correlation appears to occur between the gamma-ray and susceptibility measurements, but recovery was insufficient for a meaningful, detailed comparison.

METHODS

For this investigation, 244 samples were selected for carbonate and grain-size analyses. Between three and seven samples were taken from each of over 50 selected turbidites proportionately spaced through the turbidite sequence (1–2 turbidites/core).

Carbonate percentages were measured with a 5011 Coulometer equipped with a system 140 carbonate carbon analyzer at Texas A&M University. Carbonate samples were dried, ground, and weighed out to between 12 and 20 mg. Each sample was reacted in a 2-mL 2N HCl solution. The liberated CO_2 was reacted in a monoethanolamine solution with a colorimetric indicator to de-

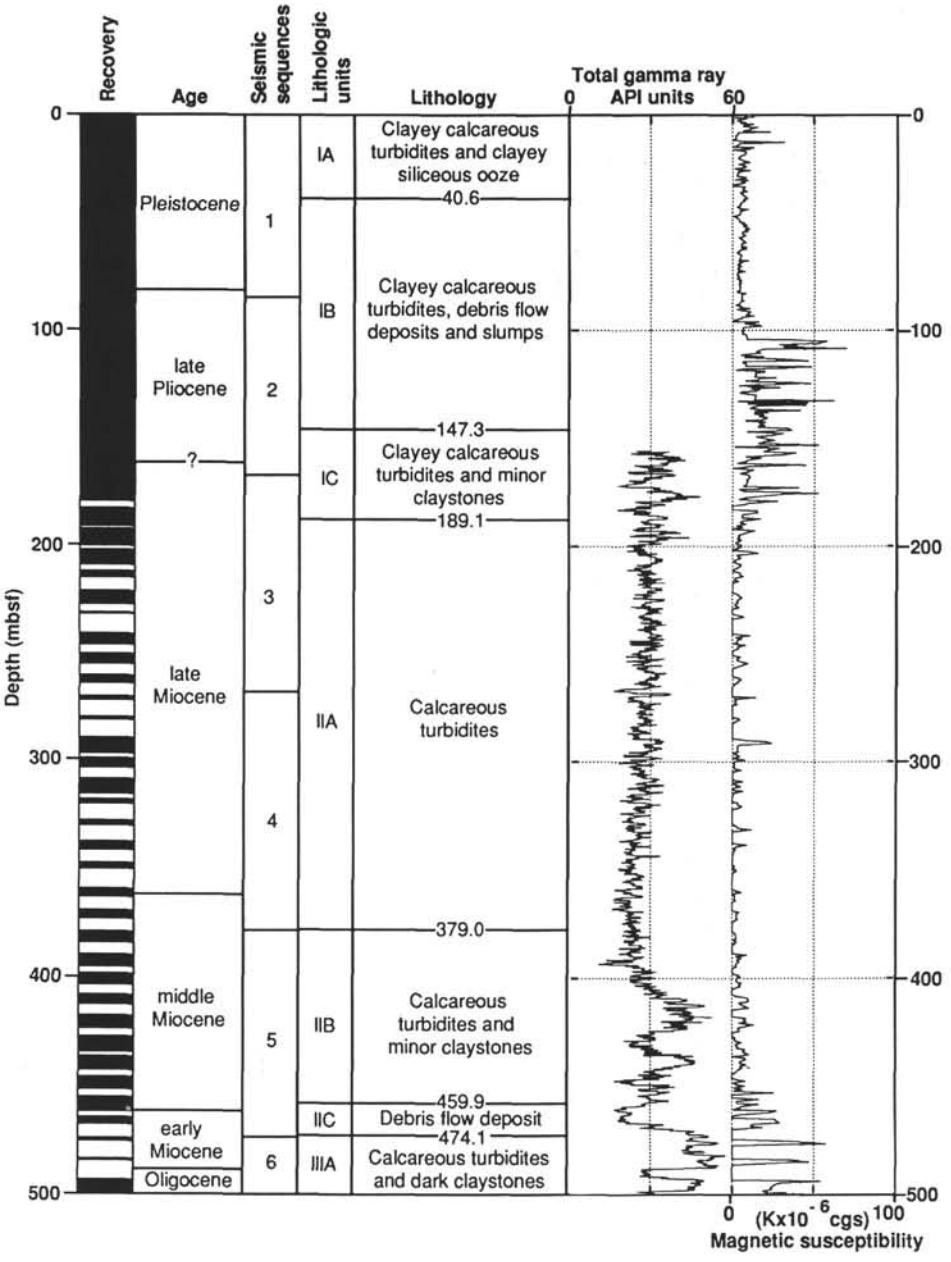

Figure 2. Site 756 Neogene synthesis chart comparing sub-bottom depths, biostratigraphic ages, seismic sequences, lithology, and magnetic susceptibility from the Site 765 chapter (Ludden, Gradstein, et al., 1990), and total gamma-ray log provided by the Borehole Research Group, Lamont-Doherty Geological Observatory.

termine the inorganic carbon content, from which the percentage of carbonate was calculated. Pure (reagent grade) carbonate standards were run twice before starting, and approximately every 15 samples thereafter. Carbonate standard percentages ranged between 99.5% and 100.5%.

Grain-size samples were weighed out to ~1.5 g and initially prepared in 50-mL graduated tubes with screw-on tops. A 30% hydrogen peroxide solution was used to initiate disaggregation for 1 hr, bringing the total volume to 5 mL (sediment + 2–3 mL peroxide). Shipboard measurements of total organic carbon throughout the turbidite sequence were typically low (<0.5%). Some of the coarsest samples were highly reactive with peroxide and required diluting. Shipboard visual core descriptions occasionally note coaly fragments within coarse turbidite bases. About 35 to 40 mL of dispersant solution was then added. A 5.5-g/L solution of sodium hexametaphosphate $(NaPO_3)_6$ was used. Samples were allowed to sit overnight. Periodically, the screw-on tops were tightened and the samples hand shaken. Just prior to grain-size analysis, each sample was placed in an ultrasonic bath for 3 min. Finally, the samples were transferred to optically transparent beakers and dispersant added, bringing the final volume to 100 mL. Grain-size analysis consisted of using both a Lasentec LAB-TEC 100 particle-size analyzer (available at Texas A&M University) and a modified pipette procedure developed for this investigation.

The LAB-TEC 100 used for the investigation is similar to the model available for use aboard the *JOIDES Resolution*. The instrument has a laser diode light source and measures the

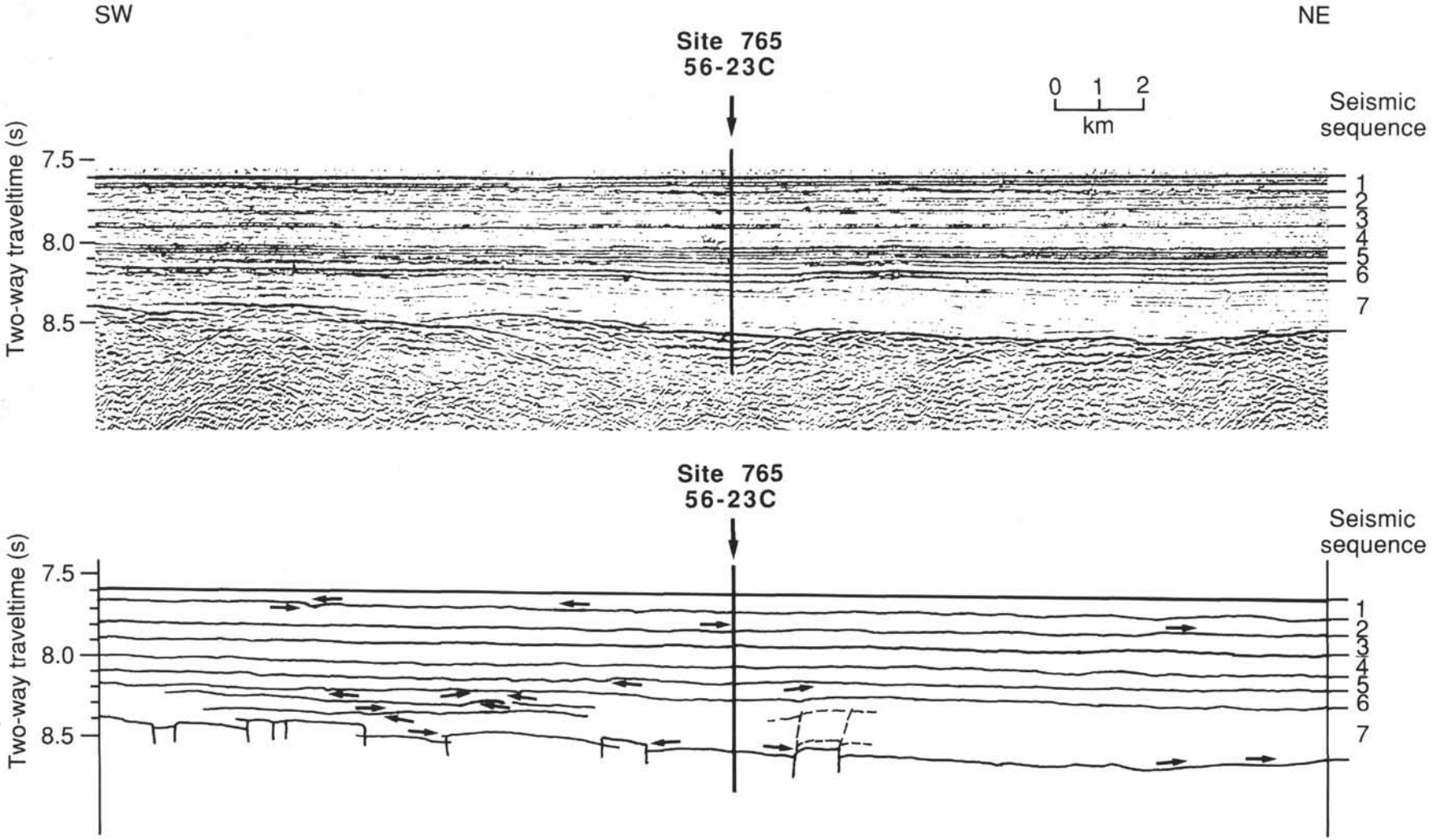

Fiure 3. BMR multifold seismic Line 56/22 across Site 765. Approximate track location is shown in Figure 1. Line drawing shows interpretation of seismic sequences 1 through 7, including disconformable relationships at sequence boundaries. From Ludden, Gradstein, et al. (1990).

backscatter of light from particles within a suspension. The suspension is maintained within a beaker that has been firmly positioned above a magnetic stirring plate. The size of a particle is determined by the length of time it takes for the particle to move across the focal point of the light beam. Data were collected from two range settings, each providing eight channels that corresponded to half ϕ-scale intervals (Table 1). The data (collected as counts per channel) were converted into percentages of the total for each setting and then were adjusted to 100% for a combined size range. Finally, the adjusted percentages were summed progressively and plotted as cumulative curves. The cumulative curves in Figure 4 are from representative coarse- and fine-grained turbidite samples analyzed at concentrations of ~5, 10, and 15 g/L. The LAB-TEC 100 provided similar results over the range of concentrations tested, but increased sample concentrations yielded slightly coarser cumulative curves. Sample concentrations of 15 g/L (corresponding to a 1.5-g sediment sample) were decided upon for this investigation to minimize experimental error associated with weighing in the modified pipette procedure.

In Figure 5, LAB-TEC 100 results are compared with traditional sieve and pipette analyses of three samples: relatively fine-, intermediate-, and coarse-grained examples. Except for the coarse end of the fine-grained sample, the LAB-TEC 100 underestimates both ends of the grain-size distribution. Traditional procedures express grain size in the weight percent of size classes. The LAB-TEC 100 detects backscatter of light, which is determined by surface area of the particles in suspension. Surface area decreases for a given sediment mass as grain size increases. Therefore, the underestimation of coarse material by the LAB-TEC 100 is expected. Leg 124 scientists (1990) pointed out that surface area abundances are more directly comparable to smear-slide determination, historically the principal method of analyzing grain size aboard both the *Glomar Challenger* and the *JOIDES Resolution*. In addition, coarser material is less likely to be suspended uniformly to the level of the light source (2.5 cm above the beaker bottom) by magnetic stirring. Underestimation of the fine end, especially the clay-sized material, is problematic because clays have a high ratio of surface area to mass. Flocculation is unlikely, as similar methods for dispersal and sediment sample concentrations were used for both LAB-TEC 100 and pipette analyses. It seems more likely that the LAB-TEC 100 is not consistently detecting clear backscatter from the fine silt- and clay-sized particles. The LAB-TEC 100 does provide a means of calibration whereby raw counts for each channel can be weighted by compensation factors, but according to Lasentec, "compensation factors may only be good for a specific material at a specific concentration," and "entering the correct compensation factors is more of an art than a science" (Lasentec Operations Manual). The use of compensation factors was not attempted for this investigation. Singer et al. (1988) compared the capability of a number of grain-size analysis instruments and found that silt-clay mixtures present the greatest analytical problem for the instruments tested.

This poses a problem. Turbidites are inherently poorly sorted, clay-rich sediments. Obviously, a procedure for providing grain-size distribution for comparison with LAB-TEC 100 results is desirable. Standard pipette procedures are time-consuming and require large samples. A modified pipette procedure employing Stokes settling velocities was developed for this investigation. Total volume of each LAB-TEC 100 sample was 100 mL, and each contained a known mass of dispersant. Following LAB-TEC 100 analysis (while the sample was still stirring and, presumably, a uniform suspension), a 20-mL aliquot was withdrawn; this represented 20% of the total sediment population and dispersant. Decanting the upper 20 mL of the sample remaining in the beaker (after sufficient time was allowed for settling out sand- and silt-sized particles) yielded 20% of the total clay population and dispersant. The remaining sample was wet-sieved through a 62-µm screen. Material remaining on the screen represented 80% of the total sand population. At this point, one could easily calculate the total sand, silt, and clay populations. This procedure worked well, except for the very coarse samples, where the abundant sand tended to clog the pipette during withdrawal of the total sediment aliquot. For these cases, the LAB-TEC samples were run at ~60 mL, after which they were wet-sieved with dispersant (~40 mL) until the sample reached 100 mL. Material remaining on the screen represented 100% of the total sand population. The sample was re-suspended in the LAB-TEC 100, and the modified pipette procedure was run for the silt and clay populations.

Bed thickness represents another important parameter for characterizing vertical sequences of turbidites. Upon recovery, cores

Table 1. Intervals of particle-size data collected using size ranges provided by Lasentec LAB-TEC 100 particle-size analyzer.

125-µm sieve		16-µm sieve	
(phi)	(µm)	(phi)	(µm)
> 3.0	>125	>6.0	>16
3.0-3.5	125-88	6.0-6.5	16-11
3.5-4.0	88-63	6.5-7.0	11-8
4.0-4.5	63-44	7.0-7.5	8-6
4.5-5.0	44-31	7.5-8.0	6-4
5.0-5.5	31-22	8.0-8.5	4-3
5.5-6.0	22-16	8.5-9.0	3-2
<6.0	<16	<9.0	<2

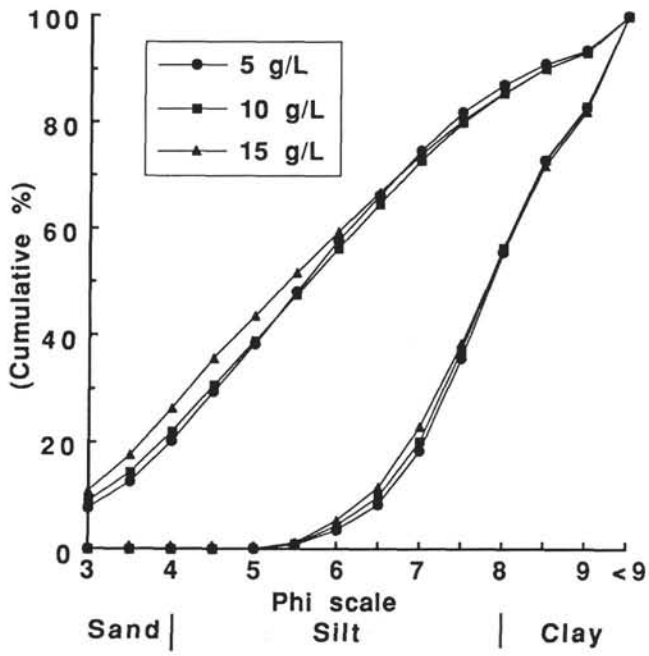

Figure 4. Cumulative percent grain-size curves of representative coarse- and fine-grained turbidite samples analyzed using Lasentec LAB-TEC 100 particle-size analyzer. Three curves for each sample represent different sample concentrations (solid circles = ~0.5 g/L, solid squares = ~1.0 g/L, solid triangles = ~1.5 g/L).

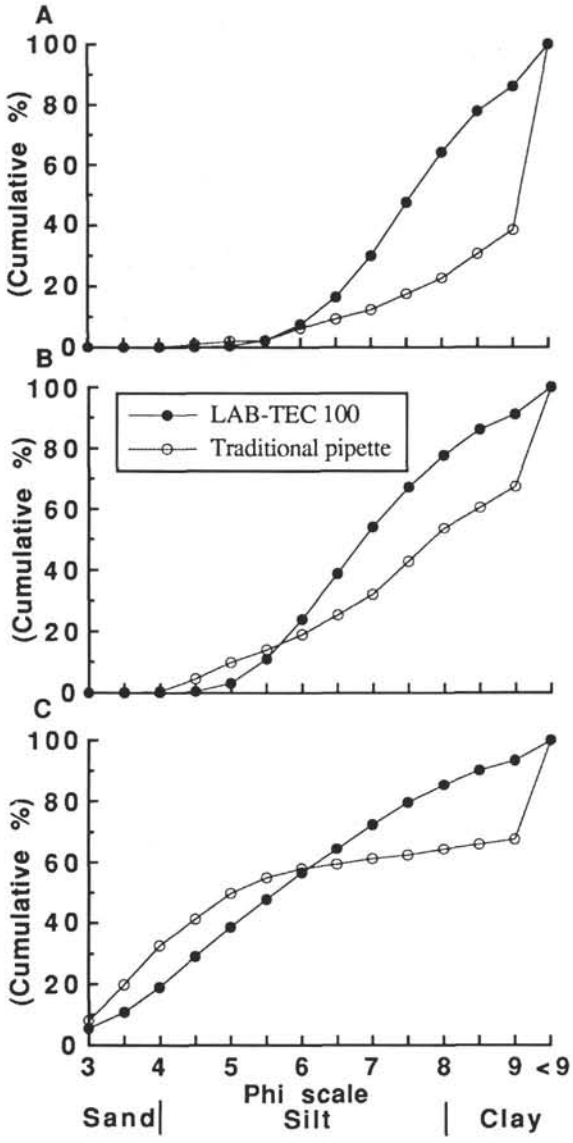

Figure 5. Cumulative percent grain-size curves of representative fine- (**A**), intermediate- (**B**), and coarse-grained (**C**) turbidite samples comparing LAB-TEC 100 results (solid circles) with standard pipette and sieve results (open circles).

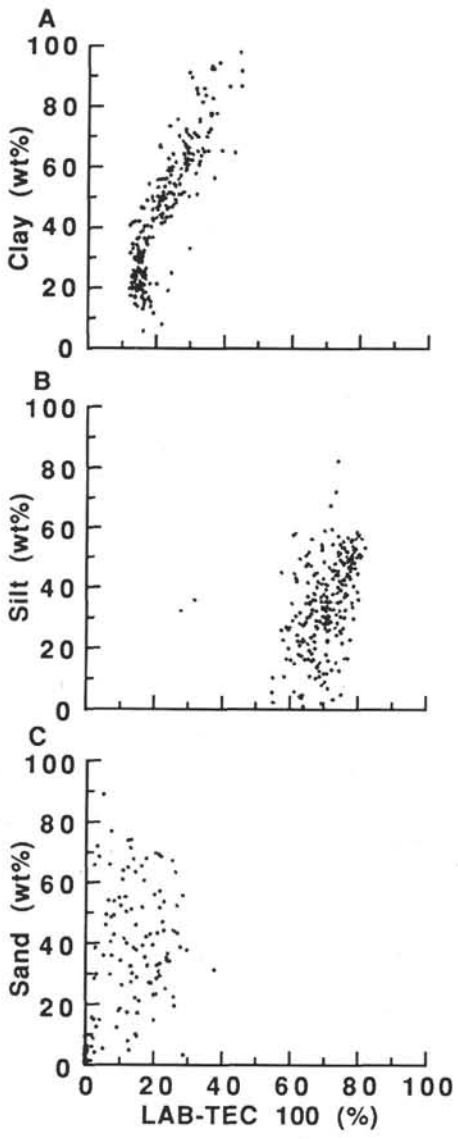

Figure 6. Scatter charts comparing percent of clay (**A**), silt (**B**), and sand (**C**) of all samples from LAB-TEC 100 and the modified pipette procedures.

brought on board the *JOIDES Resolution* were sectioned into 1.5-m lengths to provide easier handling and storage. These sections are convenient units to use when measuring bed thickness. The number of turbidites was tallied for 88 complete sections between 150 and 475 mbsf, using shipboard visual core descriptions. The turbidites/section values (bed abundance) were assigned the depth to the top of each section. Bed abundance is inversely related to average bed thickness.

Following analyses, data were compiled for the characterization of individual turbidites and for the turbidite sequence as a whole (Table 2).

RESULTS

In Figure 6, the percentages of sand, silt, and clay obtained from the LAB-TEC 100 are compared with those using the modified pipette procedure. These data are listed in Table 2. In general, a positive, but poor, correlation exists between the two procedures. The LAB-TEC 100 exhibited less response to intersample variability, over-representing the presence of silt, which is to be expected in light of comparison to standard pipette procedures (Fig. 3). The percent sand comparison shows the greatest scatter. This is attributed primarily to difficulties in maintaining the sand in uniform suspension. The LAB-TEC 100 appears most sensitive in detecting variations in clay content >~30 wt%, although the actual values were underestimated. At this point, it seems fitting to emphasize the preliminary nature of the methods applied. The scope of this investigation was concerned more with relative than with absolute variations in grain size. Originally, I planned to rely heavily on the LAB-TEC 100 results, but it was soon evident that intersample variability using the LAB-TEC 100 was insufficient without applying weighting factors. An objective and efficient approach to this problem was not readily apparent. To apply weighting factors successfully requires some prior knowledge of the sample being analyzed. Therefore, an additional method was going to be necessary to gain sufficient knowledge of the sample to apply weighting factors objectively. The modified pipette method can provide sand, silt, and clay ratios; these can be

matched by undertaking an iterative procedure for applying weighting factors to raw LAB-TEC 100 counts. However, the repeatability of the modified pipette procedure has not been thoroughly tested.

To look at textural variation through the turbidite sequence, a grain-size parameter was needed for plotting values vs. depth. The weight-percent values from the modified pipette procedure display greater intersample variation. The large amount of scatter in the sand percentage comparison (Fig. 6C) is disturbing and suggests significant experimental error in both procedures. Weight-percent clay, or conversely, cumulative weight-percent sand and silt was selected as the grain-size parameter because it exhibits the largest range of values and the least amount of scatter in the LAB-TEC 100 comparison (Fig. 6A).

Grain size varies principally within individual turbidites, but characterization of a vertical sequence relates more to variation among individual turbidites. To plot cumulative weight-percent sand and silt vs. depth in a meaningful way, I had to subdivide the data scatter that resulted from interturbidite variation. Normally, turbidites are subdivided according to a facies model (e.g., facies A, B, C, D, and E) on the basis of the primary sedimentary structures present (Bouma, 1962). The relative absence of primary sedimentary structures in Subunit IIA prevented an objective assignment within the context of a "Bouma sequence." To subdivide the data (both grain-size and carbonate values) in the depth plots, samples were assigned to upper, middle, and lower turbidite divisions, based on the spatial location of samples within the turbidites.

In Figure 7, cumulative weight-percent sand and silt and bed abundance are plotted vs. depth. Total gamma-ray and magnetic-susceptibility curves are included for reference and comparison, as with the plot of percent carbonate and bed abundance vs. depth (Fig. 8). The grain-size, carbonate, and bed-abundance data share a similar overall trend with depth.

All these data are variable in Subunit IIB. Low values of cumulative sand and silt (<15%) and carbonate (<10%) are from clay-rich pelagic intervals. Intermediate values are from the tops of turbidites into which pelagic clay has been reworked by bioturbation. From the relative distribution of upper, middle, and lower turbidite samples, fining- and less calcareous-upward trends are evident within individual turbidites. The upper turbidite samples were almost invariably the finest, but reverse grading between the middle and lower turbidite samples is not unusual.

The variability of all the data decreases over a short transition through upper Subunit IIB and lowermost Subunit IIA. From 420 to 360 mbsf, cumulative weight-percent sand and silt values increase (from 7%–75% to 44%–87%), carbonate percentages increase (from 6%–87% to 82%–92%), total gamma-ray counts decrease (from 45 to 15 API units), and magnetic-susceptibility measurements decrease (from 10 to 2 K $\times$ 10^{-6} cgs). Bed abundance decreases abruptly from 13 to 6 turbidites/1.5 m section at 360 mbsf. Each of these trends levels off somewhat, and then, at least through the upper half of Subunit IIA, gradually reverses.

Significant bedding breaks occur at 360 and 290 mbsf, where bed abundance abruptly decreases and then gradually increases upward. A bedding break at 360 mbsf corresponds to the late to middle Miocene boundary in lowermost Subunit IIA and, as described previously, represents a turning point following a short transition of grain-size, carbonate, and total gamma-ray values. A bedding break at 290 mbsf possibly ties to the boundary between seismic sequences 3 and 4 (Fig. 2) in middle Subunit IIA. This bedding break is characterized by gamma-ray and magnetic-susceptibility peaks. Carbonate values (Fig. 8) step down (60%–80% directly above vs. 72%–93% directly below) above the break. Above 290 mbsf, through upper Subunit IIA, average bed thickness (inverse of bed abundance), grain size (principally upper

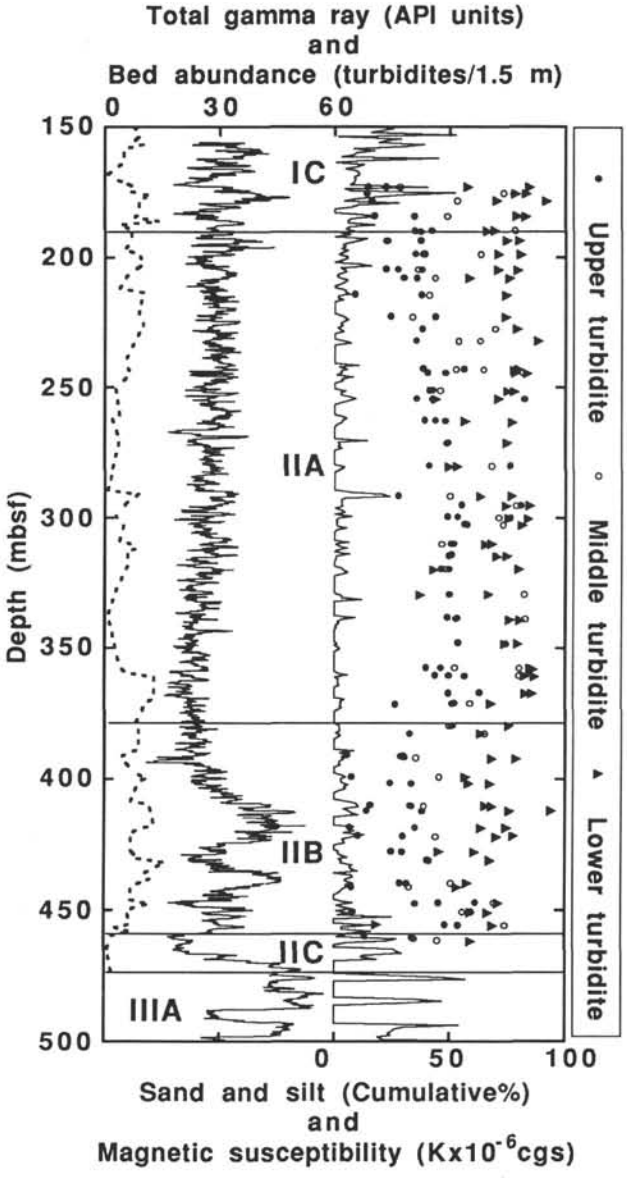

Figure 7. Bed abundance, total gamma-ray log, cumulative weight percent sand and silt (>8 ϕ from modified pipette procedure), and magnetic susceptibility plotted vs. sub-bottom depth for lithologic Subunits IC, IIA, IIB, IIC, and IIIA at Site 765 (dashed line = bed abundance); grain-size samples are from upper turbidite divisions (solid circles), middle turbidite divisions (open circles), and lower turbidite divisions (solid triangles).

turbidite), and percent carbonate gradually decrease. Total gamma-ray values gradually increase across the same interval. The data in Subunit IC are variable, which, as in lower Subunit IIB, is attributed to increased abundance of clayey pelagic intervals.

DISCUSSION

This investigation supports the idea of a late to middle Miocene turbidite depositional system having measurable evolutionary trends in bedding, grain size, and mineralogy. Stow et al. (1985) discussed the principal factors that influence the development of turbidite systems. These include sediment type and supply, tectonics, and sea level. The setting of Site 765 places

Table 2. List of core sections for/and bed-abundance measurements and core samples for/and carbonate and grain-size measurements.

Core, section, interval (cm)	Depth (mbsf)	BA	TD	CO_3 (%)	Modified pipette procedure			LAB-TEC 100		
					sand (wt%)	silt (wt%)	clay (wt%)	sand (%)	silt (%)	clay (%)
123-765B- 16H-5	150.2	8								
17H-1	153.9	9								
17H-2	155.4	8								
17H-3	156.9	10								
17H-4	158.4	5								
17H-6	161.4	5								
17H-7	162.9	5								
18H-1	163.6	5								
18H-4	168.1	1								
18H-5	169.6	2								
18H-6	171.1	5								
18H-7, 72-74	172.7		U	29.6	0.9	13.8	85.3	0.1	68.1	31.8
18H-7, 85-86	172.8		U	63.6	0.0	22.5	77.5	0.0	62.3	37.7
18H-7, 95-96	172.9		M	62.9	0.0	28.7	71.3	0.0	64.7	35.3
18H-7, 105-106	173.0		L	69.1	15.5	42.6	41.9	2.0	75.5	22.5
18H-CC, 4-5	173.1		L	71.4	73.8	10.8	15.4	12.5	68.9	18.6
19X-1	173.3	8								
19X-2	174.8	7								
19X-2, 48-49	175.3		U	3.0	0.0	14.1	85.9	0.0	68.3	31.7
19X-2, 58-59	175.4		M	65.8	55.7	17.9	26.4	20.3	62.6	17.1
19X-2, 68-69	175.5		M	75.4	56.9	21.0	22.1	21.8	62.9	15.3
19X-2, 78-79	175.6		L	78.0	68.4	14.9	16.7	22.3	61.5	16.2
19X-2, 88-89	175.7		L	66.3	65.8	12.9	21.3	7.3	72.4	20.3
19X-3	176.3	12								
19X-4	177.8	9								
19X-4, 39-40	178.2		U	10.7	0.0	16.4	83.6	0.1	65.5	34.4
19X-4, 49-50	178.3		M	61.5	0.1	53.3	46.6	0.1	75.4	24.5
19X-4, 59-60	178.4		L	58.1	69.6	1.0	29.4	20.6	64.2	15.2
19X-4, 63-64	178.4		L	7.9	88.8	3.2	8.0	5.2	72.9	21.9
20X-1	183.0	9								
20X-1, 92-93	183.9		U	25.0	0.0	17.4	82.6	0.0	63.5	36.5
20X-1, 102-103	184.0		U	77.9	0.0	34.8	65.2	0.0	60.6	39.4
20X-1, 112-113	184.1		M	76.6	3.5	45.7	50.8	0.1	72.5	27.4
20X-1, 122-123	184.2		L	71.9	35.3	44.1	20.6	17.6	67.2	15.2
20X-1, 136-137	184.4		L	57.4	67.1	16.1	16.8	25.6	60.4	14.0
20X-2	184.5	8								
20X-3	186.0	14								
20X-4	187.5	4								
20X-5	189.0	7								
20X-5, 54-55	189.5		U	83.0	0.3	42.0	57.7	0.0	68.3	31.7
20X-5, 64-65	189.6		U	81.7	0.0	34.9	65.1	0.0	64.7	35.3
20X-5, 74-75	189.7		M	85.9	30.5	47.9	21.6	21.6	65.4	13.0
20X-5, 84-85	189.8		L	81.3	32.6	37.1	30.3	18.4	65.4	16.2
20X-5, 94-96	189.9		L	80.2	42.7	23.6	33.7	19.1	66.3	14.6
20X-5, 102-103	190.0		U	24.0	9.3	28.2	62.5	0.2	71.2	28.6
21X-1	192.7	7								
21X-1, 64-65	193.3		U	58.0	9.3	28.2	62.5	0.0	70.5	29.5
21X-1, 74-75	193.4		U	55.1	0.2	22.3	77.5	0.0	63.7	36.3
21X-1, 84-85	193.5		M	54.9	0.0	23.1	76.9	0.0	63.9	36.1
21X-1, 94-95	193.6		L	60.2	7.5	67.4	25.1	12.7	71.8	15.5
21X-1, 103-104	193.7		L	63.5	33.1	47.2	19.7	22.0	64.7	13.3
21X-2	195.7	6								
21X-3	197.2	5								
21X-4	198.7	9								
21X-4, 134-136	198.5		U	77.9	0.4	34.7	64.9	0.0	65.9	34.1
21X-4, 146-147	198.7		U	75.7	0.7	37.9	61.4	0.0	67.3	32.7

significant constraints on these factors. Site 765 exists on a mature, starved, passive margin. Low subsidence rates within the receiving basin, broad sheer widths, and low continental-margin gradients are all attributes characteristic of this setting.

Seismic activity tends to influence the frequency and volume of sediment gravity flows. Mature, massive margins typically experience infrequent, but large, earthquakes that trigger infrequent, but massive, slope failures. Frequent seismic activity along active margins generates more regular, but smaller, events. The major tectonic element of the region is the convergent plate boundary along the Sunda-Banda Arc. Site 765 is distant, but was probably influenced by earthquakes generated at the convergence zone. The Australian margin experienced a progressive collision with the Sunda-Banda Arc during the Miocene through Pliocene. It also seems logical that the degree of tectonic influence would increase as the collision progressed.

The profound effect of Neogene glacio-eustatic fluctuations on terrigenous deep-sea sedimentation is well documented, but the nature of the response for calciclastic margins is less clear. Shanmugam et al. (1985) saw a correlation of both siliciclastic and calciclastic turbidites with lowstands of sea level throughout the rock record. Alternatively, Droxler and Schlager (1985) suggested that, at least of active, shallow-water carbonate platforms, calciclastic turbidites are most common during highstands of sea level, when the platforms are submerged and actively producing and shedding material onto nearby slopes.

Table 2 (continued).

21X-5, 7-8	198.8		M	75.1	5.9	33.5	60.6	0.2	70.2	29.6
21X-5, 14-15	198.8		M	74.6	29.9	33.7	36.4	13.9	69.5	16.6
21X-5, 23-24	198.9		L	65.0	46.8	24.4	28.8	22.7	62.2	15.1
21X-5, 32-33	199.0		L	48.8	65.6	15.3	19.1	2.7	73.7	23.6
22X-1	202.4	10								
22X-2	203.9	9								
22X-2, 67-68	204.6		U	61.0	0.0	22.4	77.6	0.0	64.1	35.9
22X-2, 74-75	204.6		U	48.7	0.0	27.6	72.4	0.0	64.1	35.9
22X-2, 84-85	204.7		U	59.9	1.0	37.0	62.0	0.1	69.2	30.7
22X-2, 94-95	204.8		M	63.8	0.3	36.1	63.6	0.0	66.8	33.2
22X-2, 105-106	205.0		L	72.5	43.0	28.1	28.9	21.2	63.0	15.8
22X-2, 114-115	205.0		L	69.8	63.2	16.4	20.4	26.4	59.1	14.5
22X-3	205.4	7								
22X-4	206.9	6								
22X-4, 104-105	207.9		U	54.7	0.0	30.2	69.8	0.0	65.1	34.9
22X-4, 114-115	208.0		U	69.0	0.4	35.5	64.1	0.0	69.2	30.8
22X-4, 124-125	208.1		M	71.9	1.2	42.6	56.2	0.7	62.1	37.2
22X-4, 134-135	208.2		L	73.1	14.5	44.2	41.3	4.3	74.2	21.5
22X-4, 145-146	208.4		L	67.7	74.0	2.0	24.0	13.4	69.6	17.0
23X-1	212.1	4								
23X-2	213.6	10								
23X-2, 79-80	214.4		U	75.0	0.0	8.9	91.1	0.0	70.4	29.6
23X-2, 89-90	214.5		U	73.2	0.0	37.8	62.2	0.0	70.1	29.9
23X-2, 99-100	214.6		M	72.2	0.4	40.9	58.7	0.0	71.1	28.9
23X-2, 108-109	214.7		L	75.8	41.9	32.8	25.3	17.9	66.5	15.6
24X-1	221.8	9								
24X-1, 96-97	222.8		U	72.2	0.0	24.5	75.5	0.0	67.3	32.7
24X-1, 102-103	222.8		U	74.1	0.0	44.0	56.0	0.1	76.8	23.1
24X-1, 112-113	222.9		M	70.4	0.0	33.9	66.1	0.0	71.0	29.0
24X-1, 122-123	223.0		L	77.1	24.9	49.5	25.6	23.6	63.0	13.4
24X-2	223.3	10								
24X-4	226.3	10								
24X-4, 106-107	227.4		U	71.6	0.0	38.2	61.8	0.0	67.1	32.9
24X-4, 166-117	227.5		M	79.0	28.6	41.3	30.1	15.2	69.5	15.4
24X-4, 123-124	227.5		L	62.3	67.6	11.7	20.7	14.1	70.1	15.8
25X-1, 49-50	232.0		U	61.3	0.1	35.5	64.4	0.0	70.4	29.6
25X-1, 59-60	232.1		M	70.9	5.1	58.3	36.6	5.3	79.7	15.0
25X-CC, 4-5	232.2		M	70.0	3.9	50.2	45.9	2.9	76.7	20.4
25X-CC, 14-15	232.3		L	77.8	71.7	16.7	11.6	3.5	77.1	19.4
26X-1	241.2	5								
26X-2	242.7	6								
26X-2, 19-20	242.9		U	52.9	0.3	38.3	61.4	0.1	74.1	25.8
26X-2, 24-25	242.9		U	73.2	1.0	55.4	43.6	0.1	75.7	24.2
26X-2, 34-35	243.0		M	78.4	4.8	48.1	47.1	0.8	78.3	20.9
26X-2, 44-45	243.1		M	80.0	12.2	52.8	35.0	3.4	79.4	17.2
26X-2, 59-60	243.3		L	86.5	28.3	51.7	20.0	21.0	65.5	13.5
26X-3, 80-81	243.5		L	79.1	52.0	26.1	21.9	26.9	59.6	13.5
26X-3	244.2	7								
26X-3, 9-10	244.3		U	77.2	3.6	37.0	59.4	0.0	71.0	29.0
26X-3, 19-20	244.4		U	79.7	1.8	46.6	51.6	0.1	71.6	28.3
26X-3, 29-30	244.5		M	73.5	65.3	16.3	18.4	16.6	67.0	16.4
26X-3, 39-40	244.6		L	78.2	60.4	18.2	21.4	17.1	66.6	16.3
26X-3, 49-50	244.7		L	64.4	60.7	18.0	21.3	10.9	70.8	18.3
26X-3, 57-58	244.8		L	60.6	71.2	12.5	16.3	13.3	68.8	17.9
27X-1	250.9	3								
27X-1, 9-10	251.0		U	62.8	0.1	42.9	57.0	0.0	72.7	27.3
27X-1, 29-30	251.2		U	70.6	0.2	41.2	58.6	0.1	75.4	24.5
27X-1, 49-50	251.4		M	73.2	0.7	45.4	53.9	0.1	74.3	25.6
27X-1, 69-70	251.6		L	81.4	21.9	53.5	24.6	14.8	69.5	15.7
27X-1, 87-88	251.8		L	67.0	55.5	22.7	21.8	28.6	58.1	13.3
27X-3, 48-49	254.4		U	61.8	0.4	35.5	64.1	0.1	75.0	24.9
27X-3, 54-55	254.4		L	85.0	37.6	45.0	17.4	29.9	57.5	12.6
27X-3, 64-65	254.5		U	59.7	0.2	42.7	57.1	0.1	75.6	24.3
27X-3, 74-75	254.6		L	79.8	16.9	54.4	28.7	15.2	69.3	15.5

The onset of abundant turbidites at Site 765 coincided with a period of progressive basinward shifts in coastal onlap (Haq et al., 1987), attributed to the build-up of the Antarctic continental ice sheet. Turbidite coarseness, carbonate content, and bed thickness increased to near-maximum values at 360 mbsf. This approximate point of the upper to middle Miocene boundary coincides with the base of the second-order TB3 supercycle (Haq et al., 1987), a major eustatic lowstand. It is unclear how a eustatic event having a magnitude on the order of 100 m could significantly alter conditions on the Exmouth Plateau, presumably the source of the redeposited materials, which on average is more than 1500 m deep. It seems likely that increased turbidite abundance resulted from changes in oceanographic conditions, such as increased productivity and/or circulation, in response to the onset of glacial build-up in Antarctica. An extensive upper Oligocene to middle Miocene progradational cycle for the Northwest Australian Shelf has been described by Apthorpe (1988). Convincing evidence exists for at least two depositional episodes within the turbidite

Table 2 (continued).

Core, section, interval (cm)	Depth (mbsf)	BA	TD	CO_3 (%)	Modified pipette procedure sand (wt%)	silt (wt%)	clay (wt%)	LAB-TEC 100 sand (%)	silt (%)	clay (%)
27X-3, 79-80	254.7		L	58.5	1.2	43.0	55.8	0.5	77.8	21.7
28X-1	260.6	4								
28X-2	262.1	2								
28X-2, 40-41	262.5		U	64.5	0.0	39.4	60.6	0.0	70.7	29.3
28X-2, 63-64	262.7		U	70.0	0.0	44.1	55.9	0.0	73.4	26.6
28X-2, 88-89	263.0		M	71.1	0.3	48.1	51.6	0.1	76.0	23.9
28X-2, 114-115	263.2		L	73.9	0.7	56.2	43.1	0.7	79.3	20.0
28X-2, 134-135	263.4		L	84.0	34.1	43.1	22.8	24.1	61.8	14.1
29X-1	270.2	4								
29X-1, 111-112	271.3		U	60.0	2.5	47.0	50.5	0.2	77.7	22.1
29X-1, 119-120	271.4		M	72.1	1.4	47.6	51.0	0.7	75.8	23.5
29X-1, 128-129	271.5		L	71.7	32.2	43.0	24.8	13.5	69.9	16.6
30X-1, 18-19	280.1		U	64.6	0.5	40.9	58.6	0.1	76.5	23.4
30X-1, 28-29	280.2		U	74.3	4.5	72.0	23.5	13.0	73.4	13.6
30X-1, 38-39	280.3		M	79.9	9.8	58.8	31.4	14.9	70.2	14.9
30X-1, 52-53	280.4		L	75.3	32.2	21.4	46.4	18.3	65.4	16.3
30X-1, 69-70	280.6		L	63.9	0.0	50.0	50.0	0.4	80.7	18.9
31X-1	289.6	1								
31X-2	291.1	9								
31X-2, 44-45	291.5		U	45.2	5.6	22.2	72.2	0.2	71.1	28.7
31X-2, 54-55	291.6		M	72.3	1.7	48.7	49.6	0.2	77.0	22.8
31X-2, 64-65	291.7		L	86.5	38.3	38.7	23.0	3.1	79.9	17.0
31X-2, 67-68	291.8		L	76.0	28.3	35.1	36.6	2.8	78.2	19.0
31X-4	294.1	6								
31X-4, 104-105	295.1		U	78.0	0.0	55.4	44.6	0.1	78.0	21.9
31X-4, 114-115	295.2		U	89.5	36.4	44.6	19.0	24.3	61.3	14.4
31X-4, 124-125	295.3		M	89.7	51.4	27.7	20.9	21.8	63.8	14.4
31X-4, 134-135	295.4		L	93.0	52.0	32.8	15.2	10.4	72.9	16.7
31X-4, 144-145	295.5		L	90.9	48.9	25.8	25.3	8.5	74.8	16.7
32X-1	299.3	3								
32X-1, 11-12	299.4		U	79.2	0.0	49.2	50.8	0.0	74.8	25.2
32X-1, 39-40	299.7		U	78.9	0.7	53.0	46.3	0.5	79.3	20.2
32X-1, 60-61	299.9		M	87.4	17.1	54.4	28.5	12.4	72.6	15.0
32X-1, 79-80	300.1		M	88.2	19.2	57.3	23.5	26.2	60.9	12.9
32X-1, 97-98	300.3		L	84.2	43.9	31.8	24.3	23.1	62.9	14.0
32X-1, 122-123	300.5		L	88.8	53.6	30.5	15.9	8.4	74.9	16.7
32X-2	300.8	4								
32X-3	302.3	5								
32X-3, 14-15	302.4		U	82.1	0.0	56.6	43.4	0.0	77.0	23.0
32X-3, 33-34	302.6		U	79.3	0.6	57.3	42.1	0.5	80.4	19.1
32X-3, 54-55	302.7		M	86.2	20.9	52.5	26.6	15.8	69.4	14.8
32X-3, 70-71	303.0		L	73.4	76.8	4.8	18.4	7.6	75.3	17.1
33X-1	309.0	4								
33X-1, 89-90	309.9		U	72.8	0.2	50.7	49.1	0.0	74.3	25.7
33X-1, 99-100	310.0		U	73.7	0.0	51.9	48.1	0.0	74.2	25.8
33X-1, 109-110	310.1		M	73.3	0.5	46.4	53.1	0.2	79.2	20.6
33X-1, 120-121	310.2		L	83.5	9.1	59.4	31.5	15.2	72.3	12.5
33X-1, 132-133	310.3		L	83.9	35.1	30.7	34.2	23.9	61.7	14.4
33X-2	310.5	8								
33X-3	312.0	8								
33X-4	313.5	6								
33X-4, 64-65	314.1		U	81.5	0.3	50.8	48.9	0.1	78.1	21.8
33X-4, 84-85	314.3		U	79.3	1.7	48.1	50.2	0.4	79.1	20.5
33X-4, 104-105	314.5		M	88.1	22.9	47.1	30.0	20.1	66.2	13.7
33X-4, 124-125	314.7		L	93.8	48.3	26.7	25.0	7.6	75.7	16.7
33X-4, 138-139	314.9		L	91.2	37.5	33.1	29.4	15.1	69.5	15.4
34X-1	318.7	6								
34X-1, 74-75	319.4		U	57.6	0.1	46.6	53.3	0.1	77.3	22.6
34X-1, 84-85	319.5		U	71.3	0.3	49.8	49.9	0.1	77.8	22.1
34X-1, 94-95	319.6		M	76.7	0.3	48.3	51.4	0.1	75.5	24.4
34X-1, 104-105	319.7		L	86.3	22.2	58.0	19.8	26.1	61.6	12.3
34X-1, 118-119	319.9		L	40.0	68.2	6.8	25.0	4.1	71.3	24.6
35X-1	328.3	3								
35X-1, 103-104	329.3		U	77.2	0.5	49.7	49.8	0.2	78.5	21.3

depositional system. A significant break, particularly in bed-abundance and carbonate data, occurs within the upper Miocene at 290 mbsf in proximity to a regional seismic sequence boundary. As mentioned previously, no obvious change in lithology occurs, but recovery across this interval is poor, and useful information is surely missing. Retrogradation of the turbidite depositional system seems to have accompanied rising sea level through the lower half of the TB3 supercycle. Five third-order eustatic cycles (Haq et al., 1987) occurred during the upper Miocene and lower Pliocene, but individual responses to the third-order cycles were not recognized.

Concomitant with retrogradation of the turbidite depositional system, from the latest Miocene into the Pliocene–Pleistocene is increasing occurrence and magnitude of massive slope failures. The oldest record of such events is that of single turbidites in the uppermost Miocene, up to 630 cm thick, and with intraformational conglomerates at their base. The largest such deposit in the Pliocene is more than 42.5 m thick and consists of a single turbidite

Table 2 (continued).

	35X-1, 114-115	329.4		M	77.8	53.4	29.2	17.4	23.1	60.9	16.0
	35X-1, 124-125	329.5		L	87.0	26.9	40.1	33.0	18.8	68.0	13.2
	35X-1, 134-135	329.6		L	89.4	4.8	32.6	62.6	0.1	76.3	23.6
	36X-1	337.9	1								
	36X-1, 31-32	338.2		U	86.6	1.3	47.9	50.8	0.0	73.3	26.7
	36X-1, 51-52	338.4		U	81.1	0.2	53.2	46.6	0.1	76.1	23.8
	36X-1, 71-72	338.6		M	83.4	1.0	51.9	47.1	0.1	77.0	22.9
	36X-1, 104-105	338.9		M	90.8	54.8	28.3	16.9	10.0	74.0	16.0
	36X-1, 140-141	339.3		L	80.2	50.1	26.2	23.7	12.1	71.7	16.2
	36X-2, 5-6	339.5		L	43.8	64.8	15.9	19.3	12.5	71.4	16.1
	37X-1, 44-45	347.9		U	86.8	2.0	52.0	46.0	0.2	76.6	23.2
	37X-1, 64-65	348.1		M	92.0	17.6	57.0	25.4	9.8	74.2	16.0
	37X-1, 84-85	348.3		L	92.9	29.1	50.6	20.3	22.0	64.7	13.3
	37X-1, 99-100	348.5		L	80.1	34.0	40.1	25.9	10.4	74.2	15.4
	38X-1	357.1	4								
	38X-1, 32-33	357.4		U	65.6	1.0	39.1	59.9	0.1	75.1	24.8
	38X-1, 39-40	357.5		U	76.5	1.0	45.5	53.5	0.0	74.2	25.8
	38X-1, 50-51	357.6		M	80.8	1.3	51.3	47.4	0.1	74.9	25.0
	38X-1, 59-60	357.7		M	92.2	35.8	44.7	19.5	7.9	76.9	15.2
	38X-1, 69-70	357.8		L	88.5	69.1	16.3	14.6	21.6	64.4	14.0
	38X-1, 79-80	357.9		L	91.8	55.0	31.1	13.9	11.7	73.6	14.7
	38X-1, 93-94	358.0		L	87.2	53.7	32.5	13.8	6.8	74.6	18.6
	39X-1, 26-27	367.0		U	68.1	5.8	57.5	36.7	2.0	80.1	17.9
	39X-1, 36-37	367.1		U	80.3	1.3	48.5	50.2	0.1	70.1	29.8
	39X-1, 65-66	367.4		L	94.0	35.7	50.3	14.0	5.4	78.1	16.5
	39X-1, 79-80	367.5		L	95.6	29.5	53.7	16.8	3.4	78.6	18.0
123-765C-	2R-1	359.6	6								
	2R-1, 68-70	360.3		U	81.8	0.3	43.8	55.9	0.1	77.6	22.3
	2R-1, 79-80	360.4		U	82.4	3.3	46.6	50.1	0.1	78.0	21.9
	2R-1, 89-90	360.5		U	84.7	1.0	55.8	43.2	0.1	78.2	21.7
	2R-1, 99-100	360.6		M	92.0	26.1	54.3	19.6	10.8	74.8	14.4
	2R-1, 119-120	360.8		L	92.3	26.7	56.1	17.2	19.5	66.4	14.1
	2R-1, 128-130	360.9		L	89.6	67.7	19.3	13.0	17.9	65.8	16.3
	2R-2	361.1	13								
	3R-1	369.3	13								
	3R-2	370.8	11								
	3R-2, 14-15	370.9		U	76.8	1.0	51.5	47.5	0.5	78.7	20.8
	3R-2, 24-25	371.0		U	75.4	1.2	50.2	48.6	1.1	79.7	19.2
	3R-2, 34-35	371.1		M	89.4	14.6	44.7	40.7	20.1	67.5	12.4
	3R-2, 49-50	371.3		L	86.3	39.1	29.1	31.8	16.9	67.8	15.3
	3R-2, 53-54	371.3		U	9.0	4.9	21.8	73.3	0.6	75.5	23.9
	4R-1	379.0	8								
	4R-1, 63-64	379.6		U	79.4	1.5	50.0	48.5	0.6	78.5	20.9
	4R-1, 71-72	379.7		M	75.0	1.0	49.2	49.8	0.6	77.4	22.0
	4R-1, 83-84	379.8		L	85.0	33.9	42.0	24.1	24.8	62.1	13.1
	4R-2	380.5	9								
	4R-3, 63-64	382.6		U	51.4	3.2	29.8	67.0	0.2	78.7	21.1
	4R-3, 74-75	382.7		M	80.2	38.5	27.0	34.5	28.0	58.9	13.1
	4R-3, 84-85	382.8		L	81.5	43.9	19.9	36.2	25.9	59.6	14.5
	5R-1	388.6	9								
	5R-2	390.1	7								
	5R-2, 73-74	390.8		U	4.2	0.0	5.7	94.3	0.0	61.4	38.6
	5R-2, 102-103	391.1		U	57.8	2.8	27.4	69.8	0.0	67.7	32.3
	5R-2, 134-135	391.4		U	57.8	0.0	29.0	71.0	0.0	68.9	31.1
	5R-3	391.6	4								
	5R-3, 4-5	391.6		M	59.3	0.0	30.6	69.4	0.0	69.6	30.4
	5R-3, 34-35	391.9		M	62.4	2.7	33.0	64.3	0.0	71.9	28.1
	5R-3, 74-75	392.3		L	83.3	39.8	28.8	31.4	12.2	72.1	15.7
	5R-3, 87-88	392.5		L	86.1	50.9	28.2	20.9	13.5	69.9	16.6
	6R-1	398.3	9								
	6R-1, 85-86	399.2		U	5.0	3.0	4.7	92.3	0.0	63.9	36.1
	6R-1, 95-96	399.3		M	80.1	0.0	45.8	54.2	0.0	73.0	27.0
	6R-1, 105-106	399.4		L	82.3	6.1	51.0	42.9	0.6	80.4	19.0
	6R-2	399.8	11								

overlying a debris-flow deposit also overlying a slumped unit. The onset of massive slope failures was possibly coincidental to the progressive Miocene–Pliocene collision between the Australian margin and the Sunda-Banda Arc (Carter et al., 1976), but they are more likely interrelated.

ACKNOWLEDGMENTS

I would like to acknowledge the combined efforts of the Shipboard Scientific Party, the ODP technical and logistics staff, and the crew of *JOIDES Resolution* toward the successful completion of Leg 123 and publication of the indispensable Leg 123 *Initial Reports*. The Borehole Research Group, Lamont-Doherty Geological Observatory, is commended for their prompt transmittal of requested logging data.

The Department of Oceanography and Ocean Drilling Program, both at Texas A&M University, provided the facilities for this investigation. H. Jensvold contributed excellent technical support for the shore-based analyses.

Reviews by R. Hesse and S. O'Connell greatly improved this manuscript. Thanks go to A. Meyer for additional review and discussion. An editorial review by S. Stewart was extremely valuable. Finally, I acknowledge the diligence of F. Gradstein, the Editorial Review Board member assigned to this chapter.

Table 2 (continued).

Core, section, interval (cm)	Depth (mbsf)	BA	TD	CO_3 (%)	Modified pipette procedure sand (wt%)	silt (wt%)	clay (wt%)	LAB-TEC 100 sand (%)	silt (%)	clay (%)
6R-3	401.3	9								
6R-3, 33-34	401.6		U	42.0	0.0	24.4	75.6	0.0	73.8	26.2
6R-3, 44-45	401.7		U	59.6	0.0	33.7	66.3	0.3	78.5	21.2
6R-3, 54-55	401.8		M	87.5	16.9	41.1	42.0	15.5	70.6	13.9
6R-3, 64-65	401.9		L	82.9	23.1	35.3	41.6	20.9	66.0	13.1
6R-3, 74-75	402.0		L	92.7	42.6	25.2	32.2	8.4	75.1	16.5
7R-1	408.0	7								
7R-2	409.5	11								
7R-2, 59-60	410.1		U	8.2	5.8	10.1	84.1	0.2	67.8	32.0
7R-2, 69-70	410.2		U	57.5	3.1	30.2	66.7	0.0	71.3	28.7
7R-2, 76-77	410.3		U	84.4	3.3	30.4	66.3	0.0	70.3	29.7
7R-2, 89-90	410.4		M	68.7	3.6	35.5	60.9	0.0	71.6	28.4
7R-2, 97-98	410.5		L	77.1	49.0	16.7	34.3	6.2	76.3	17.5
7R-2, 108-109	410.6		L	80.3	45.7	22.9	31.4	6.0	77.8	16.2
7R-3	411.0	12								
7R-3, 114-115	412.1		U	9.5	3.4	10.8	85.8	0.0	66.0	34.0
7R-3, 126-127	412.3		U	61.9	3.0	35.3	61.7	0.0	71.1	28.9
7R-3, 135-136	412.4		L	93.1	12.0	82.2	5.8	9.4	74.1	16.5
7R-3, 143-144	412.4		L	90.3	63.7	12.6	23.7	11.0	74.7	14.3
8R-1	417.7	13								
8R-1, 101-102	418.4		U	5.9	3.2	3.7	93.1	0.0	63.6	36.4
8R-1, 114-115	418.5		U	61.7	2.8	32.5	64.7	0.0	70.6	29.4
8R-1, 124-125	418.6		L	86.9	63.2	11.7	25.1	14.6	71.0	14.4
8R-1, 135-136	418.8		L	73.7	41.3	22.7	36.0	11.4	71.2	17.4
8R-2	419.2	9								
8R-3	420.7	7								
8R-3, 113-114	421.5		U	19.1	2.6	8.0	89.4	0.1	69.6	30.3
8R-3, 134-135	421.7		L	81.1	40.3	37.6	22.1	7.6	77.0	15.4
8R-3, 135-136	421.8		U	50.6	3.2	26.8	70.0	0.0	73.3	26.7
8R-4, 4-5	421.9		M	67.8	3.9	40.5	55.6	0.6	78.8	20.6
8R-4, 29-30	422.2		L	86.0	43.8	26.9	29.3	26.2	60.0	13.8
9R-1	427.3	7								
9R-1, 25-26	427.6		U	41.5	2.9	22.2	74.9	0.0	67.3	32.7
9R-1, 32-33	427.6		U	61.7	3.0	26.7	70.3	0.0	68.1	31.9
9R-1, 42-43	427.7		M	58.3	3.1	26.6	70.3	0.0	70.4	29.6
9R-1, 52-53	427.8		L	64.4	9.6	36.2	54.2	1.8	80.2	18.0
9R-1, 62-63	427.9		L	71.1	45.8	15.3	38.9	14.9	69.0	16.1
9R-2	428.8	8								
9R-3	430.3	8								
9R-3, 43-44	430.7		U	64.2	2.8	37.9	59.3	0.0	72.7	27.3
9R-3, 52-53	430.8		U	62.1	3.6	37.0	59.4	0.1	76.2	23.7
9R-3, 63-64	430.9		M	65.4	3.3	38.2	58.5	0.1	76.4	23.5
9R-3, 73-74	431.0		L	82.8	32.2	35.4	32.4	13.3	71.8	14.9
9R-3, 83-84	431.1		L	81.1	38.3	29.5	32.2	14.3	70.8	14.9
9R-4	431.8	16								
10R-1	436.5	10								
10R-2	438.0	12								
10R-3, 0-1	439.5		U	28.6	3.1	25.7	71.2	0.0	71.1	28.9
10R-3, 10-11	439.6		U	61.6	2.7	29.0	68.3	0.0	72.1	27.9
10R-3, 20-21	439.7		M	62.0	1.2	49.9	48.9	1.8	80.9	17.3
10R-3, 30-31	439.8		L	59.6	27.1	30.9	42.0	13.6	71.3	15.1
10R-4	441.0	7								
10R-4, 11-12	441.1		U	20.8	3.6	4.2	92.2	0.1	63.1	36.8
10R-4, 22-23	441.2		M	57.1	2.6	30.2	67.2	0.0	71.4	28.6
10R-4, 33-34	441.3		L	70.2	18.3	35.2	46.5	10.3	74.1	15.6
11R-1	446.0	7								
11R-1, 101-102	447.0		U	80.6	8.5	53.1	38.4	2.4	82.1	15.5
11R-1, 110-111	447.1		U	75.5	3.6	42.1	54.3	0.1	74.6	25.3
11R-1, 122-123	447.2		M	80.1	39.2	30.5	30.3	19.9	65.8	14.3
11R-1, 146-147	447.5		L	73.2	51.5	20.0	28.5	16.7	67.4	15.9
11R-1, 149-150	447.5		U	2.7	3.0	32.4	64.6	28.9	27.9	43.2
11R-2	447.5	12								
11R-3	449.0	8								
11R-4	450.5	6								

Funding for my post-cruise research was provided by JOI-USSAC and was administered by the Texas A&M Research Foundation.

REFERENCES

Apthorpe, M., 1988. Cainozoic depositional history of the North West Shelf. *In* Purcell, P. G., and Purdell, R. R. (Eds.), *The North West Shelf, Australia*. Proc. Pet. Expl. Soc. Aust. Symp., 55–84.

Bouma, A. H., 1962. *Sedimentology of some Flysch Deposits:* Amsterdam (Elsevier).

Carter, D. J., Audley-Charles, M. G., and Barber, A. J., 1976. Stratigraphical analysis of island arc-continental margin collision in eastern Indonesia. *J. Geol. Soc. London*, 132:179–198.

Droxler, A. W., and Schlager, W., 1985. Glacial versus interglacial sedimentation rates and turbidity frequency in the Bahamas. *Geology*. 13:799–802.

Table 2 (continued).

11R-4, 7-8	450.6		U	0.4	3.0	5.4	91.6	0.0	55.0	45.0
11R-4, 18-19	450.7		U	84.4	3.7	56.1	40.2	0.3	81.1	18.6
11R-4, 29-30	450.8		M	82.8	3.2	52.8	44.0	0.1	78.7	21.2
11R-4, 39-40	450.9		L	74.8	14.7	44.7	40.6	2.6	80.0	17.4
11R-4, 49-50	451.0		L	83.2	31.0	35.9	33.1	38.0	32.0	30.0
12R-1	455.2	7								
12R-1, 31-32	455.5		L	46.6	2.9	15.8	81.3	0.0	66.5	33.5
12R-1, 41-42	455.6		U	69.5	2.8	45.7	51.5	0.0	77.9	22.1
12R-1, 51-52	455.7		U	77.1	3.9	50.3	45.8	0.1	81.0	18.9
12R-1, 61-62	455.8		M	86.6	32.6	41.7	25.7	21.1	65.3	13.6
12R-1, 71-72	455.9		L	72.9	43.1	26.0	30.9	27.1	57.6	15.3
12R-2	456.7	3								
12R-3	458.2	7								
12R-4	459.7	2								
12R-4, 18-19	459.9		U	13.7	3.0	10.6	86.4	0.0	58.5	41.5
12R-4, 69-70	460.4		U	52.9	2.7	31.4	65.9	0.0	66.3	33.7
12R-4, 119-120	460.9		U	53.4	2.6	32.4	65.0	0.0	67.8	32.2
12R-5, 19-20	461.4		M	61.9	2.6	42.7	54.7	0.0	76.1	23.9
12R-5, 70-71	461.9		L	63.5	29.5	30.1	40.4	7.4	76.1	16.5
13R-1	464.6	1								

BA = bed abundance (turbidites/1.5 m section); TD = turbidite division (U = upper turbidite, M = middle turbidite, L = lower turbidite); CO_3 = carbonate analysis.

Haq, B. U., Hardenbol, J., and Vail, P. R., 1987. Chronology of fluctuating sea-levels since the Triassic. *Science*, 235:1156–1167.

Haq, B. U., von Rad, U., O'Connell, S., et al., 1990. *Proc. ODP. Init. Repts.*, 122: College Station, TX (Ocean Drilling Program).

Lasentec Operations Manual for the LAB-TEC 100 Particle Size Analyzer: Bellevue, WA (Laser Sensor Technology, Inc.).

Ludden, J. N., Gradstein, F. M., et al., 1990. *Proc. ODP, Init. Repts.*, 123: College Station, TX (Ocean Drilling Program).

Shanmugam, G., Moiola, R. J., and Damuth, J. E., 1985. Eustatic control of submarine fan development. *In* Bouma, A. H., Norman, W. R., and Barnes, N. E. (Eds.), *Submarine Fans and Related Turbidite Systems:* New York (Springer-Verlag), 23–28.

Shipboard Scientific Party, 1990. Explanatory notes. *In* Rangin, C., Silver, E. A., von Breymann, M. T., et al., *Proc. ODP, Init. Repts.*, 124: College Station, TX (Ocean Drilling Program), 7–34.

Singer, J. K., Anderson, J. B., Ledbetter, M. T., McCave, I. N., Jones, K.P.N., Wright, R., 1988. An assessment of analytical techniques for the size analysis of fine-grained sediments. *J. Sediment. Petrol.*, 58:534–543.

Stow, D.A.V., Howell, D. G., Nelson, C. H., 1985. Sedimentary, tectonic, and sea-level controls. *In* Bouma, A. H., Norman, W. R., and Barnes, N. E. (Eds.), *Submarine Fans and Related Turbidite Systems:* New York (Springer-Verlag), 15–22.

Date of initial receipt: 18 July 1990
Date of acceptance: 21 March 1991
Ms 123B-147

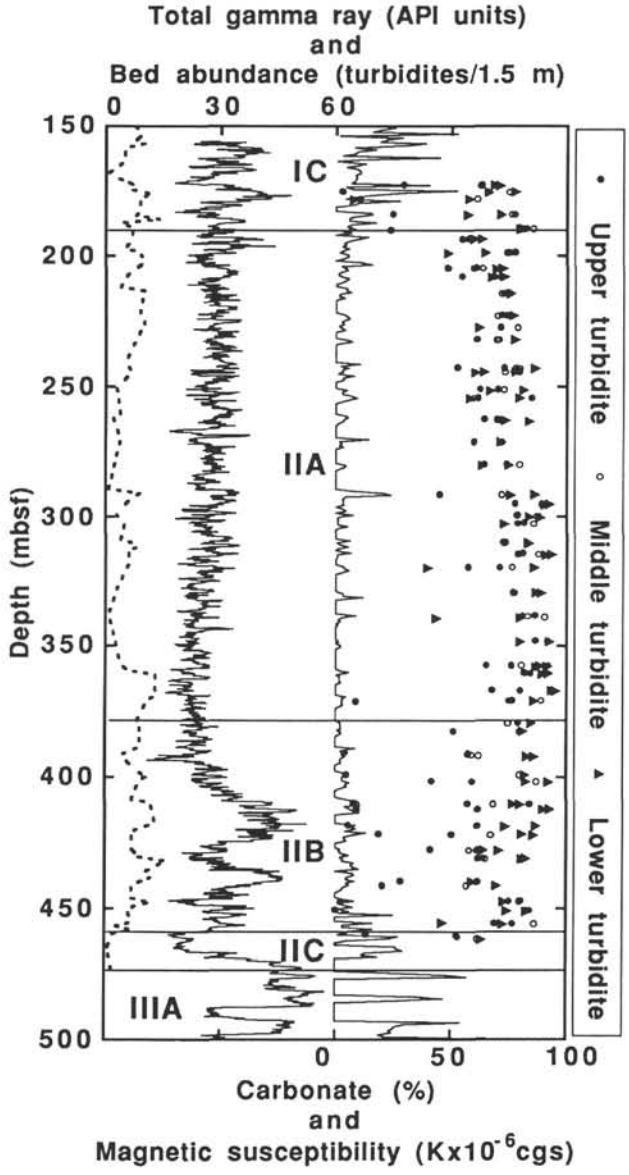

Figure 8. Bed abundance, total gamma-ray log, carbonate percent, and magnetic susceptibility plotted vs. sub-bottom depth for lithologic Subunits IC, IIA, IIB, IIC, and IIIA at Site 765 (dashed line = bed abundance). Carbonate samples are from upper turbidite divisions (solid circles), middle turbidite divisions (open circles), and lower turbidite divisions (solid triangles).